

RSC Advances



This is an *Accepted Manuscript*, which has been through the Royal Society of Chemistry peer review process and has been accepted for publication.

Accepted Manuscripts are published online shortly after acceptance, before technical editing, formatting and proof reading. Using this free service, authors can make their results available to the community, in citable form, before we publish the edited article. This *Accepted Manuscript* will be replaced by the edited, formatted and paginated article as soon as this is available.

You can find more information about *Accepted Manuscripts* in the [Information for Authors](#).

Please note that technical editing may introduce minor changes to the text and/or graphics, which may alter content. The journal's standard [Terms & Conditions](#) and the [Ethical guidelines](#) still apply. In no event shall the Royal Society of Chemistry be held responsible for any errors or omissions in this *Accepted Manuscript* or any consequences arising from the use of any information it contains.

Synthesis, Characterization, Electrochemical Properties and Catalytic Reactivity of the N-Heterocyclic Carbene-Containing Diiron Complexes

Yanhong Wang^{1,2}, Tianyong Zhang^{1,2*}, Bin Li^{1,2*}, Shuang Jiang^{1,2}, Liao Sheng^{1,2}

¹ School of Chemical Engineering and Technology, Tianjin Key Laboratory of Applied Catalysis Science and Technology, Tianjin University, Tianjin 300072, China.

² Collaborative Innovation Center of Chemical Science and Engineering (Tianjin), Tianjin 300072, China.

*Corresponding Author

E-mail: Tianyong Zhang: tyzhang@tju.edu.cn

Bin Li: libin@tju.edu.cn

Abstract:

$(\mu\text{-dmedt})[\text{Fe}(\text{CO})_3]_2$ (**I**, dmedt = 2,3-butanedithiol) was chosen as the parent complex. A series of new model complexes, N-heterocyclic carbene (NHC) substituted $(\mu\text{-dmedt})[\text{Fe-Fe}]\text{-NHC}$ (**II**, $(\mu\text{-dmedt})[\text{Fe}(\text{CO})_2]_2[\text{I}_{\text{Me}}(\text{CH}_2)_2\text{I}_{\text{Me}}]$, $\text{I}_{\text{Me}} = 1\text{-methylimidazol-2-ylidene}$; **III**, $\{(\mu\text{-dmedt})[\text{Fe}_2(\text{CO})_5]\}_2[\text{I}_{\text{Me}}(\text{CH}_2)_2\text{I}_{\text{Me}}]$; **IV**, $(\mu\text{-dmedt})[\text{Fe}_2(\text{CO})_5]\text{IMes}$, $\text{IMes} = 1,3\text{-bis}(2,4,6\text{-trimethylphenyl})\text{imidazol-2-ylidene}$; **V**, $(\mu\text{-dmedt})[\text{Fe}_2(\text{CO})_5]\text{IME}$, $\text{IME} = 1,3\text{-dimethylimidazol-2-ylidene}$) as mimics of the $[\text{Fe-Fe}]\text{-H}_2\text{ases}$ active site were synthesized from **I** and characterized by solution IR spectra, NMR spectra, elemental analysis and single-crystal X-ray diffraction. The electrochemical properties of complexes **I-V** and with HOAc were investigated by cyclic voltammetry in coordinating solvent CH_3CN to evaluate the effects of different NHC ligands on the redox properties of the iron atoms of the series complexes. It is concluded that all the new complexes are electrochemical catalysts for proton reduction to hydrogen. The symmetrically substituted cisoid basal/basal coordination complex **II** displays the most negative reduction potential own to its stronger δ -donating ability of NHC and the orientation of the NHC donor carbon as a result of the constraints of the bridging bidentate ligands. A new application for the $[\text{Fe-Fe}]\text{-NHC}$ model complexes in the directly catalytic hydroxylation of benzene to phenol was also studied. Under the optimized experimental conditions (**II**, 0.01 mmol; benzene, 0.1 mL; CH_3CN , 2.0 mL; H_2O_2 , 6.0 mmol; 60 °C, 3 h), the maximal phenol yield is 26.7%.

Keywords:

Diiron enzymes, Diiron complexes, N-heterocyclic carbene, Electrochemical properties, Catalytic hydroxylation

Introduction

Hydrogenase enzymes, which were found in a variety of microorganisms and could efficiently catalyze the reduction of protons to hydrogen, can be classified into [Fe]-H₂ases (Hmd H₂ases), [Ni-Fe]-H₂ases and [Fe-Fe]-H₂ases (H-Cluster). While, chemists are interested in studying the biomimetic chemistry of [Fe-Fe]-H₂ases, due to its highest and fastest catalytic capability for production of hydrogen among all of the three¹. Moreover, [Fe-Fe]-H₂ases is the most amenable to small molecule model studies because of its resemblance to well known organometallic complexes of the type $(\mu\text{-SR})_2[\text{Fe}^{\text{I}}(\text{CO})_2\text{L}]_2$ ². To date, diiron models, $(\mu\text{-pdt})[\text{Fe}(\text{CO})_3]_2$ (pdt = 1,3-propanedithiolato), $(\mu\text{-edt})[\text{Fe}(\text{CO})_3]_2$ (edt = 1,2-ethanedithiolato), $(\mu\text{-adt})[\text{Fe}(\text{CO})_3]_2$ (adt = 2-azapropane-1,3-dithiolato), $(\mu\text{-odt})[\text{Fe}(\text{CO})_3]_2$ (odt = oxadithiolate) and $(\mu\text{-tdt})[\text{Fe}(\text{CO})_3]_2$ (tdt = thiodithiolate), and their derivatives have been extensively studied both structures and functional mimics of the enzyme active site.

N-Heterocyclic carbenes (NHCs) are electronic, steric tunable and stable with a range of transition metal complexes. NHCs can activate some bonds (C-H, C-C and C-N) at the N atom functionalities in the presence of transition metals³. Moreover, the iron atoms combined with NHCs are more electron-rich and more easily to accept proton for the catalytic H₂ production due to the strong δ -electron-donating with negligible π -electron-accepting ability and great potential of NHCs^{3b,4}. The powerful ligands used for the designs of diiron systems are listed in Figure 1⁵.

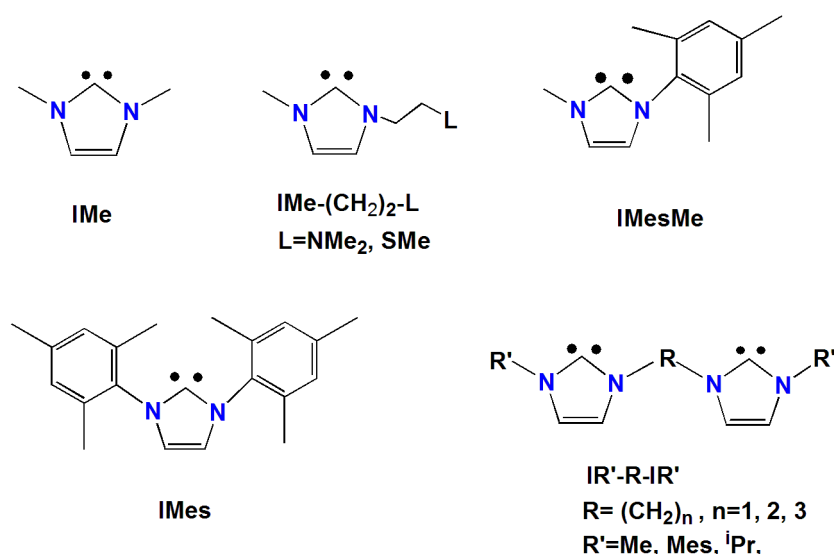
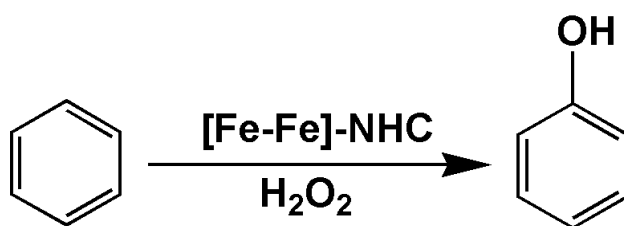


Figure 1. The widely used NHCs in diiron model complexes.

Herein, we chose $(\mu\text{-dmedt})[\text{Fe}(\text{CO})_3]_2$ ($\text{dmedt} = 2,3\text{-butanedithiol}$) as the parent complex due to its greater durability upon electrochemical cycling⁶. Donovan⁶ synthesized complex **I** by the reaction of iron dodecacarbonyl with 2,3-butanedithiol. However, we used iron pentacarbonyl reacted with 2,3-butanedithiol to yield the same complex **I**⁷. Typical NHC ligands of IMe , IMes and $\text{IMe}(\text{CH}_2)_2\text{IMe}$ which are different with each other in structure were chosen to synthesis NHC-containing $[\text{Fe-Fe}]\text{-H}_2\text{ases}$ models. The main purposes for such study are: (i) To prepare the first NHC-containing $[(\mu\text{-dmedt})\text{Fe}_2(\text{CO})_6]$ models, both monosubstituted and disubstituted model complex were included; (ii) To examine the influences of different NHC ligands upon the structures and properties of the NHC-containing complexes.

Iron complexes containing NHC ligands as homogeneous catalyst firstly used in 2000 are becoming highly attractive and challenging⁸. Then various organic transformations catalyzed by Fe-NHC have been achieved, including hydrosilylation reactions⁹, aryl Grignard–alkyl halide cross-coupling reactions¹⁰, Kumada-type alkyl–alkyl cross-coupling reactions¹¹ and ring-opening polymerization¹² etc. However, $[\text{Fe-Fe}]\text{-NHC}$ has only been used for reduction of protons to hydrogen by now¹³. In order to study the catalytic reactivity of $[\text{Fe-Fe}]\text{-NHC}$ complexes, directly hydroxylation of benzene to phenol via Scheme 1 by the series of NHCs substituted diiron complexes in mild conditions was investigated.



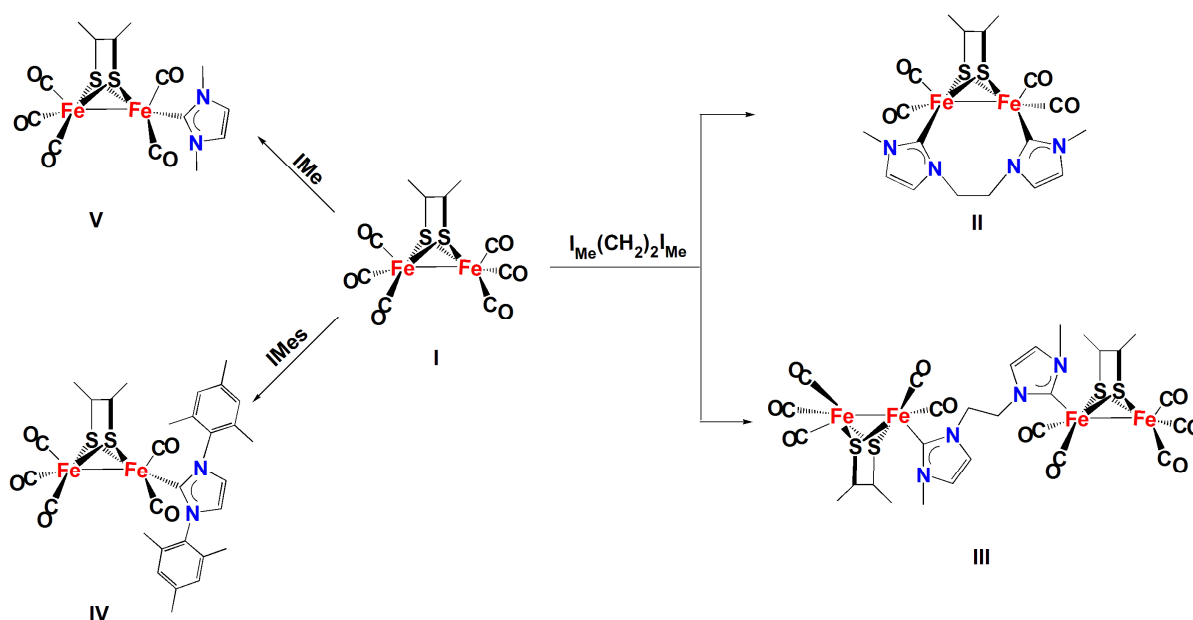
Scheme 1. Directly hydroxylation of benzene to phenol by [Fe-Fe]-NHC complexes.

Results and Discussion

Synthesis and Characteristics of the Diiron Complexes

Imidazolium salt $[\text{I}_{\text{Me}}(\text{CH}_2)_2\text{I}_{\text{Me}}]\cdot 2\text{HBr}$ (**1**), $\text{IMes}\cdot\text{HCl}$ (**2**) and $\text{IMe}\cdot\text{HI}$ (**3**) which are easily deliquescent white solid were prepared with high yields as previously reported^{4a, 14}. The ethidene-bridged imidazolium salt $[\text{I}_{\text{Me}}(\text{CH}_2)_2\text{I}_{\text{Me}}]\cdot 2\text{HBr}$ was characterized by ^1H NMR that shows a singlet at 8.84 ppm for protons of the two NCHN units in its bridged two imidazole rings.

Mono- and bi-NHCs substituted complexes were synthesized by the facile reaction of all-carbonyl complex **I** (Scheme 2) with corresponding imidazolium salt and strong base *t*-BuOK in THF at room temperature under sufficient stir and monitored by solution IR spectra. All the new model complexes could be handled in air and stored in the atmospheric conditions for a couple of weeks, due to both solids and solutions of these complexes are relatively stable to air and water and are not hygroscopic.



Scheme 2. Synthetic route of complexes **II-V**.

The IR spectra of the five complexes displayed three or four absorption bands in the range 2073-1886 cm^{-1} (Figure 2) for their terminal carbonyls in CH_2Cl_2 . The bands of **II-V** are considerably shifted towards lower energy compared to those of their parent complex **I**, which is obviously due to their CO ligands being substituted by stronger electron-donating NHC ligands. Previous studies state that iron atoms become more electron-rich and more easily to accept proton for the catalytic H_2 production after the hexacarbonyl parent complex is substituted by stronger δ -donating ligands^{5b, 15}. As a result, the stronger back-bonding from the metal to the CO ligands is formed, then the $\nu_{\text{C=O}}$ absorbance bands shift towards lower frequencies. So, we estimate that the $\nu_{\text{C=O}}$ bands can be considered as a useful indicator for evaluating the variation in the electron density of the Fe atoms. However, the electron donating capacity of bidentate dimer $\text{I}_{\text{Me}}(\text{CH}_2)_2\text{I}_{\text{Me}}$ which conjuncts with two iron of an [Fe-Fe] active center is obviously much higher than that of monodentate dimer, IMes or IMe, mainly due to not only the presence of the more electronegative nitrogen atom in the latter two ligands, but also the orientation of the NHC donor carbon as a result of the constraints of the bridging bidentate ligands.

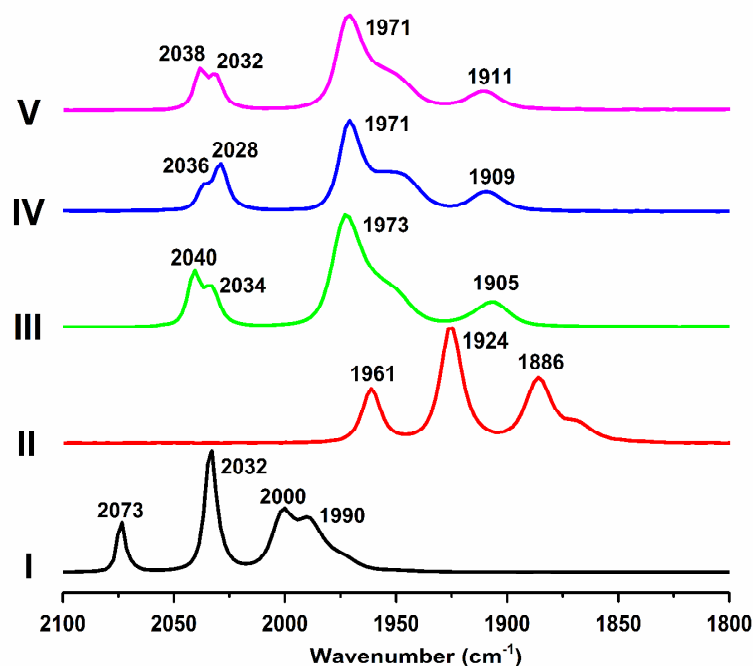


Figure 2. The $\nu(\text{CO})$ region of IR spectra of complexes **I-V** (observed in CH_2Cl_2 solution).

Interestingly, 2 equiv. of imidazolium salt **1** reacted with 7.2 equiv. *t*-BuOK in THF at room temperature followed by treatment of the resulting mixture with 1 equiv. parent complex **I** to ensure the complex **I** completely transformed. The chetaled bidentate NHC substituted model complex **II** and di-NHC ligand substituted **III** were afford in low yields (Scheme 2) which were isolated after purification by aluminum oxide chromatography. However, no complex similar with the configuration of **II** was produced in the similar studies made by Morvan^{4c} and Song¹⁶. It demonstrates that the bridged dithiolate cofactors in $(\mu\text{-dmedt})[\text{Fe}(\text{CO})_3]_2$, $(\mu\text{-pdt})[\text{Fe}(\text{CO})_3]_2$ (pdt = 1,3-propanedithiolate) and $[(\mu\text{-SCH}_2)_2(\text{Nbu-}t)][\text{Fe}(\text{CO})_3]_2$ play a key role for production of such two types of model complexes. The IR spectrum of **II** is very close to those reported for the bis-cyanide complex $[(\mu\text{-pdt})\text{Fe}_2(\text{CN})_2(\text{CO})_4]^{2-}$ (1965, 1924, 1884 cm^{-1})^{2b, 17}, but shift to lower frequencies than those of the disubstituted IMe complex $[(\mu\text{-pdt})\text{Fe}_2(\text{CO})_4(\text{IMe})_2]$ (1967, 1926, 1888 cm^{-1})^{5a} and the bis-phosphine complex $[(\mu\text{-pdt})\text{Fe}_2(\text{CO})_4(\text{PMe}_3)_2]$ (1979, 1940, 1898 cm^{-1})¹⁸. These IR data demonstrate that the bidentate $\text{I}_{\text{Me}}(\text{CH}_2)_2\text{I}_{\text{Me}}$ ligand exhibits better electron-donating ability relative to that of CN, IMe and PMe_3 . In addition, the IR spectrum of **III** displays almost the same pattern in the

carbonyl region at the very similar frequencies of monosubstituted complexes **IV** and **V**, which suggests that **III** is also a monosubstituted complex^{4c}.

Although we have tried our best, the single crystals of complexes **III** and **V** suitable for X-ray detection were not achieved. The structures of complexes **II** and **IV** were confirmed by X-ray analyses of single crystals obtained by hexane-dichloromethane solution in low temperature, and the selected bond lengths and angles are given in Table 1 and 2. The Fe₂S₂ skeleton of the two complexes shares the well-known butterfly conformation in which each iron center adopts distorted square-pyramidal coordination geometry. The two Fe atoms of complex **II** (Figure 3) are bridged by bi-NHC ligand with a symmetrically chelated cisoid basal/basal coordination pattern and adopt a distorted square-pyramidal geometry. The Fe-Fe bond distance in **II** (2.5952(6) Å) is shorter than that of the same NHC substituted model complex **A** (Figure 5) (2.6253(4) Å) made by Morvan^{4c}, but is longer than that of complex **IV** (Figure 4) (2.5870(12) Å). The Fe-C bond distances of the carbonyl of the {Fe(CO)₂NHC} subunits (**II**, 1.7490(3) Å; **IV**, 1.7540(7) Å) are significantly shorter than those of the carbonyl of the parent complex **I**, which are in the range 1.7887(19)-1.8090(2) Å⁷. This indicates an enhanced Fe-CO π -back-donation from the Fe center to the C_{carbene}^{4b, 19}. The Fe-C_{carbene} bond distances are typical of bonds having σ character^{4b, 19}. The Fe-C_{carbene} bond length of **II** (1.991(3) Å, 1.969(3) Å) are shorter than that of complex **IV** (2.000(6) Å) own to the relatively large space steric effect of the IMes ligand substituent^{5a}.

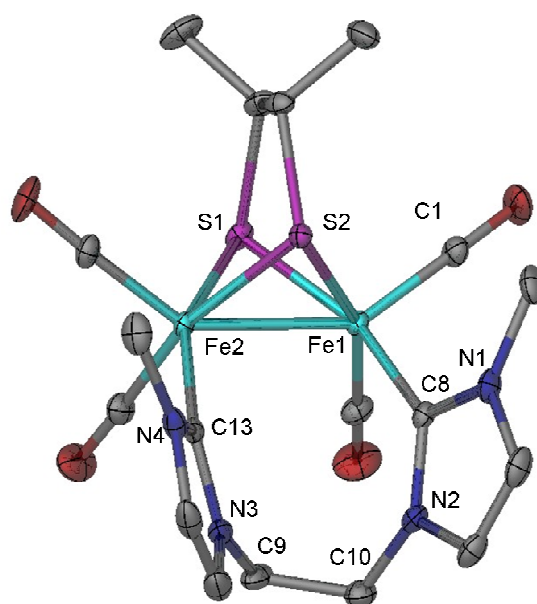


Figure 3. X-ray crystal structures of the complex **II** (ellipsoids at 30% probability level). The hydrogen atoms are omitted for clarity.

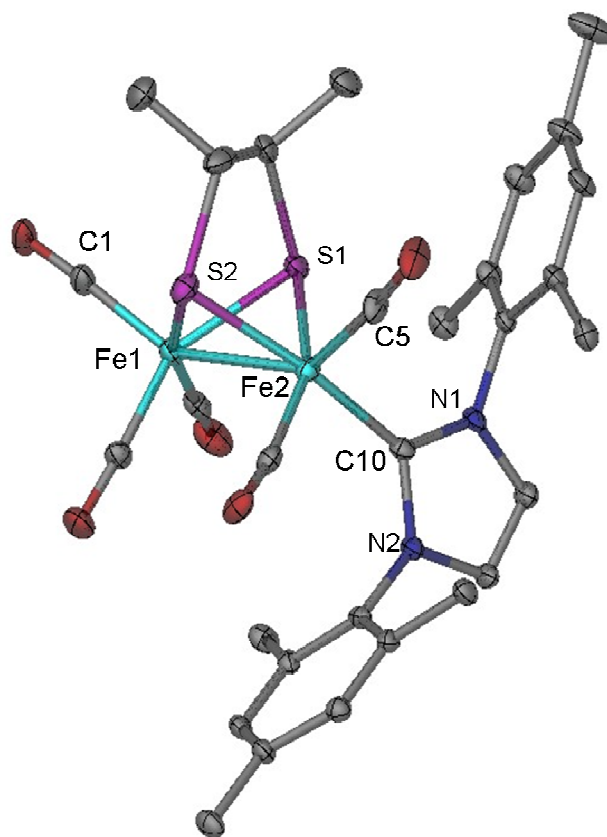


Figure 4. X-ray crystal structures of the complex **IV** (ellipsoids at 30% probability level). The hydrogen atoms are omitted for clarity.

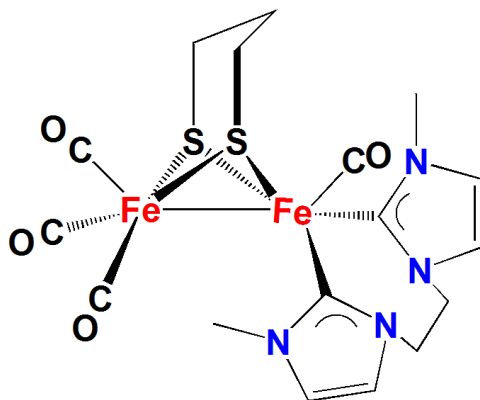


Figure 5. Structure of complex A.

Table 1. Selected bond lengths (Å) for complexes II and IV.

	II	IV
Fe(1)- Fe(2)	2.5952(6)	2.5870(12)
Fe(1)-S(1)	2.2474(8)	2.2450(18)
Fe(1)-S(2)	2.2503(8)	2.2510(19)
Fe(2)-S(1)	2.2471(8)	2.2504(17)
Fe(2)-S(2)	2.2381(8)	2.2452(19)
Fe(1)-C(1)	1.7490(3)	1.8000(8)
Fe(1)-C(8)	1.9910(3)	----
Fe(2)-C(5)	----	1.7540(7)
Fe(2)-C(10)	----	2.0000(6)
Fe(2)-C(13)	1.9690(3)	----

Table 2. Selected bond angles (Deg) for complexes **II** and **IV**.

	II	IV
S(1)-Fe(1)-S(2)	79.36(3)	78.88(7)
S(1)-Fe(1)-Fe (2)	54.73(2)	54.97(5)
S(2)-Fe(1)-Fe (2)	54.46(2)	54.77(5)
S(2)-Fe(2)-S(1)	79.62(3)	78.89(7)
S(2)-Fe(2)-Fe (1)	54.90(19)	54.98(5)
S(1)-Fe(2)-Fe (1)	54.74(2)	54.77(5)
Fe(1)-S(1)-Fe (2)	70.54(2)	70.27(6)
Fe(1)-S(2)-Fe (2)	70.65(2)	70.25(6)
N(1)-C(10)-N(2)	--	101.90(5)
N(1)-C(8)-N(2)	103.10(2)	--
N(3)-C(13)-N(4)	103.70(2)	--
N(2)-C(9)-C(10)	115.80(2)	--
N(3)-C(10)- C(9)	113.90(3)	--

Notably, in the crystal structures of complex **IV** (Figure 4), the plane of the IMes ligand twists to a large extent for reduce steric interactions with the surrounding CO ligands. The IMes group in complex **IV** lies in a basal position in accordance with $(\mu\text{-dmpdt})[\text{Fe}(\text{CO})_3][\text{Fe}(\text{CO})_2\text{IMes}]$ ($\nu_{\text{CO}} = 2030, 1971, 1947, 1913 \text{ cm}^{-1}$, in THF) and $(\mu\text{-depdt})[\text{Fe}(\text{CO})_3][\text{Fe}(\text{CO})_2\text{IMes}]$ ($\nu_{\text{CO}} = 2025, 1971, 1946, 1911 \text{ cm}^{-1}$, in THF)²⁰, but in contrast with apical positions of the same ligand in $(\mu\text{-pdt})[\text{Fe}(\text{CO})_3][\text{Fe}(\text{CO})_2\text{IMes}]$ ($\nu_{\text{CO}} = 2035, 2027, 1969, 1947, 1916 \text{ cm}^{-1}$, in THF)²¹ and $(\mu\text{-odt})[\text{Fe}(\text{CO})_3][\text{Fe}(\text{CO})_2\text{IMes}]$ ($\nu_{\text{CO}} = 2039, 1969, 1947, 1924 \text{ cm}^{-1}$, in KBr)¹⁶. It is probably states that there is a strong steric repulsion between IMes and dithiolate cofactor when the steric bulk is added to the bridgehead carbons of $\mu\text{-SRS}$. But this different dithiolate cofactor does not drastically change the thiolate donor ability according to the IR data.

Cyclic Voltammograms

The electrochemical properties of complexes **I-V** and with HOAc (Acetic acid) were investigated by cyclic voltammetry (CV) in coordinating solvent CH_3CN in the presence of Bu_4NPF_6 as supporting electrolyte (Figure 6). The redox potentials (referenced to $\text{Fc}/\text{Fc}^+ = 0.00 \text{ V}$) of **I-V** are given in Table 3 and

assigned according to the previous reports^{4c, 21-22}.

Table 3. Redox potentials of the complexes **I-V**.

Complex	E_{pc}/V vs. Fc/Fc^+	E_{pc}/V vs. Fc/Fc^+
	$E: Fe^I Fe^I \rightarrow Fe^0 Fe^0$	$Fe^I Fe^I \rightarrow Fe^{II} Fe^I$ $Fe^{II} Fe^I \rightarrow Fe^{II} Fe^{II}$
I	-1.73 ^a	0.93
	-2.23 ^b	--
II	-2.57	-0.11
		0.86
III	-2.14	0.38
		0.75
IV	-2.18 ^c	0.14
		0.95
V	-2.17	0.28
		0.71

a: $E_1: Fe^I Fe^I \rightarrow Fe^0 Fe^I$; **b:** $E_2: Fe^0 Fe^I \rightarrow Fe^0 Fe^0$; **c:** $Fe^I Fe^I(IMes)^0 \rightarrow Fe^0 Fe^I(IMes)^{-1}$.

The hexacarbonyl parent **I** has a quasi-reversible and an irreversible reduction event at ca. -1.73 V and -2.23 V. It is obviously that the electrocatalysis occurs at the second reduction potential that corresponds to an $Fe^0 Fe^0$ species in the presence of HOAc. The $Fe^{II}-H^-$ specie that results from oxidative addition of a proton to $Fe^0 Fe^0$ is set up to accept another proton, generating an $(\eta^2-H_2)Fe^{II}-Fe^0$ complex. This process is accounted for EECC (E = Electrochemical, C = Chemical) mechanism^{6, 23}.

However, a typical similar characteristic can be observed from the CVs that all members of the series display a two-electron reduction event at ca. -2.57, -2.14, -2.18 and -2.17 V, respectively. These events are shifted in a cathodic direction by ca. 860, 430, 470 and 460 mV for **II-V**, respectively, as compared to that of the first reduction event of **I**. These shifts consistent with the increase in electron density at the diiron centers as CO were replaced by the better electron donor of NHC ligands. Moreover, **II** appears at the most negative potentials among the known diiron complexes because the two basal CO of **I** have been

substituted by the better electron donor ligand $I_{Me}(CH_2)_2I_{Me}$. The reduction potential of **III**, **IV** and **V** under CV conditions is very similar to each other, which is consistent with the similarity in electron density readily observed in the CO region of IR spectrum (Figure 2). It suggests that the introduction of the bidentate NHC ligand bridged with two Fe atoms exerts a stronger influence on the redox potentials of diiron complexes than the introduction of monodentate carbene.

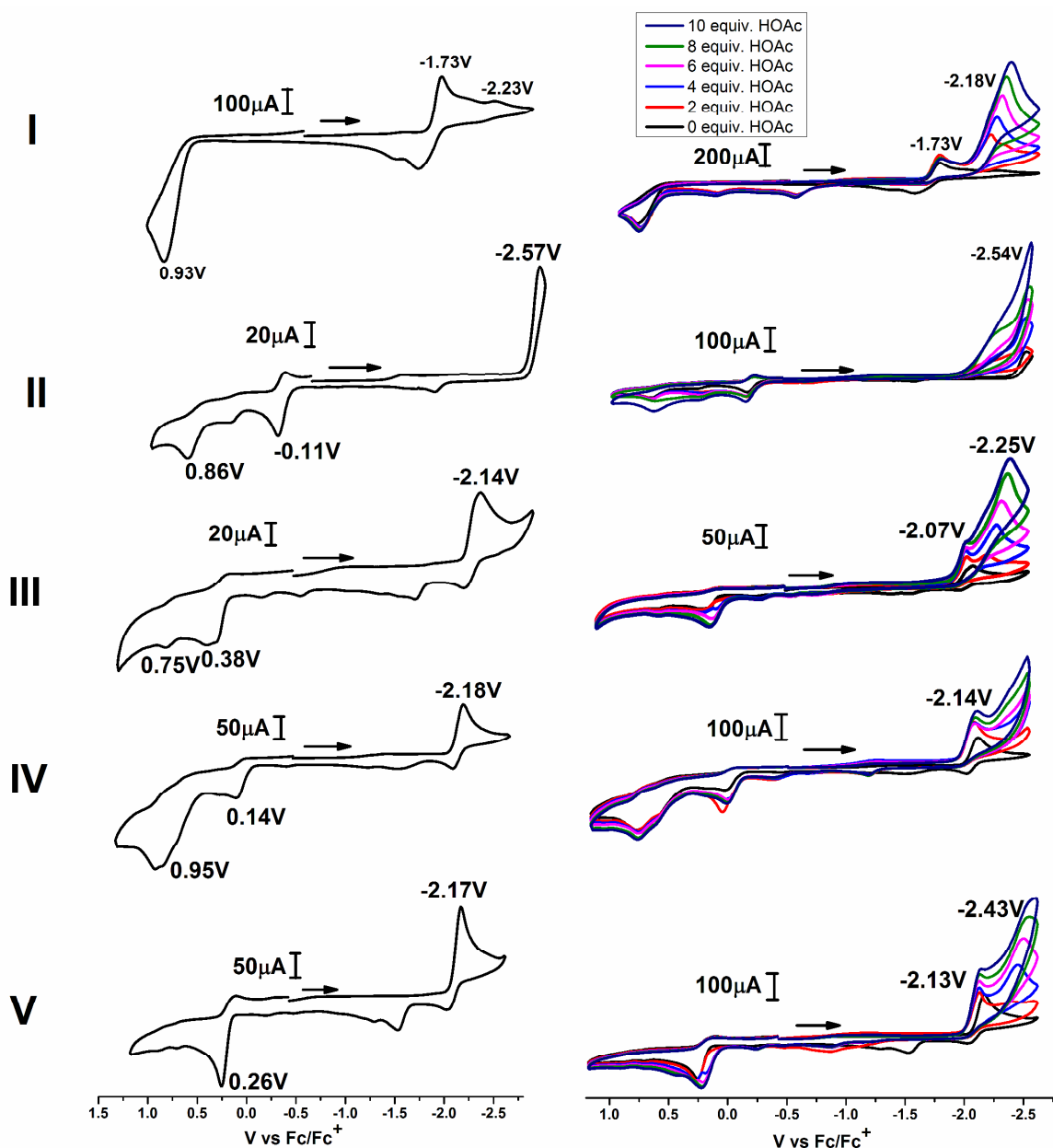


Figure 6. Cyclic voltammograms of the complexes and with HOAc (2, 4, 6, 8 and 10 equiv.) in CH_3CN solution (0.1 M

n-Bu₄NPF₆) under N₂ at room temperature: (a) **I**, 2 mM; scan rate, 200 mV/s; (b) **II**, 2 mM; scan rate, 100 mV/s; (c) **III**, 1 mM (Poor solubility); scan rate, 100 mV/s; (d) **IV**, 2 mM; scan rate, 200 mV/s; and (e) **V**, 2 mM; scan rate, 200 mV/s. All potentials are scaled to Fc/Fc⁺=0.00 V.

A quasi-reversible two-electron reduction Fe^IFe^I→Fe⁰Fe⁰ couple at ca. -2.14 and -2.17 V is observed in the CVs of complexes **III** and **V**, respectively^{5b, 21}. Interestingly, for **III** and **V**, in the presence of HOAc, new reduction peaks are observed at the more negative peaks ca. -2.25 and -2.43 V when detected under N₂, but is not observed when the CV measurement of **V** was carried out under CO (Figure S6). So we suppose that the additional reduction event under N₂ are attributed to the Fe^IFe^I/Fe⁰Fe⁰ couple of a coordinated solvent substituted species ((μ-dmedt)[Fe-Fe](NCCH₃)) which is likely to result from a radical chain reaction initiated by the production of the radical anion process^{1b, 3a, 23c, 23d}, not because of the two-electron reduction process divided into two one-electron reduction processes. Moreover, the process of CO dissociation from the labile Fe⁰Fe⁰ radical anion was inhibited by measured in CO saturated solution^{5a}. The current height of the first reduction peak at ca. -2.07 and -2.17 V of **III** and **V** shows a slight increase with added increments of HOAc, while the second new reduction peak shows a significant electrocatalytic response, which is typical of an electrocatalytic process. This suggests that both Fe⁰Fe⁰ and [(μ-dmedt)[Fe-Fe](NCCH₃)] species can combine with protons and be active toward electrocatalytic H₂ production, but the reactivity of the later is stronger than that of the former.

The conjunction of Fe and IMes ligand valence orbital permits the uptake of two electrons at the same potential. What's more, in addition to a one-electron Fe-Fe reduction, DFT shows that the arylsubstituted NHC can accept a second electron more readily than the Fe-Fe manifold^{16, 22b}. CV of **IV** states that the two electrons process of electrocatalytic H₂ production (one electron at the Fe-Fe center and one electron on the IMes ligand) with a quasi-reversible reduction at ca. -2.18 V can be assigned to the Fe^IFe^I(IMes)⁰→Fe⁰Fe^I(IMes)⁻¹ reduction. In the presence of HOAc, the Fe⁰ of [Fe⁰-Fe^I(IMes)⁻¹]²⁻ species is protonated to afford the Fe-H species of monoanion [Fe^{II}(H)-Fe^I(IMes)⁻¹]. A second protonation and internal electron transfer from the reduced IMes ligand to the iron center result in the release of dihydrogen

and regeneration of the $\text{Fe}^{\text{I}}\text{Fe}^{\text{I}}$ starting material. On the basis of the previous reports, the electrochemical process of **IV** is also inferred as an EECC mechanism^{4c, 16, 21}.

In the presence of HOAc, the current heights of the single cathodic events in the CVs of the five complexes almost increase linearly with the concentration of HOAc (Figure S8). The steeper slope displayed by the line of current-concentration indicates greater sensitivity to acid concentration. That's to say the electrocatalytic reactions were occurred^{23c, 23d}.

Catalytic Hydroxylation

Our previous study indicated that the Fe–Fe bond in the complex with the electron-donating ligand could be oxidized more easily by H_2O_2 to form the oxygen-transfer intermediate⁷. Therefore, the better electron-donating NHC ligands substituted diiron model complexes were used as the catalysts of hydroxylation of benzene.

Hydroxylation of benzene with H_2O_2 (30%, w/w, in H_2O) was carried out in a 25 mL round bottom flask equipped with a reflux condenser and a magnetic stirrer. All the experiments were conducted at ambient pressure. The blank controls (without catalyst or H_2O_2) were also conducted, and no phenol was detected.

At first, the different oxidants O_2 , H_2O_2 , PhIO, and *m*-CPBA were used as hydroxylation reagents (Table 4). The phenol yield with H_2O_2 is more than twice the *m*-CPBA under the same conditions. However, O_2 and PhIO are not able to oxidize benzene to phenol under the given experimental conditions. Thus, H_2O_2 was chosen as the oxidant in the following hydroxylation. Some parameters which would affect the phenol yield such as reaction time, temperature, amount of catalyst and H_2O_2 were also investigated (Figure S9). The temperature has a strong effect on the phenol yield. The reaction rate increases with the temperature increment, leading to a result of increased phenol yield. However, the phenol yield decreases with the further increase of temperature, which is probably partly attribute to the side reactions (Figure S11). Due to the complexity of oxidation reactions, it is hard to indentify all the by-product. Especially, some of the by-product probably could not be detected under the special GC analytic conditions. In the presence of 0.01

mmol of catalyst and 1 mmol of benzene - i.e. 100 equivalents of benzene - a yield of 25% of phenol is obtained. This means that 1 molecule of catalyst produces 25 molecules of product, which provide evidence for a catalytic process. However, adding more catalyst do not change the yield of phenol obviously, only faster. It is probably due to the reaction could be indiscriminate and give several oxidized products of which phenol is one (possibly other oxidized products have very high retention times and are not detected by GC). Figure S9 illustrates that under the optimized experimental conditions (**IV**, 0.01 mmol; benzene, 0.1 mL; CH₃CN, 2.0 mL; H₂O₂, 6.0 mmol; 60 °C; 3 h), the maximal phenol yield is 25.9%.

Table 4. Effects of different oxidants on hydroxylation of benzene to phenol^[a].

Entry	Catalyst	Oxidant	Yield (%)
1	IV	H ₂ O ₂	25.9
2	IV	<i>m</i> -CPBA	12.1
3	IV	PhIO	0
4	IV	O ₂	0

[a] catalyst, 0.01 mmol; benzene, 0.1 mL; CH₃CN, 2.0 mL; oxidant, 6.0 mmol; 60 °C; 3 h.

Complex **I** and its NHC ligands substituted derivatives were used as homogeneous catalysts to catalyze the hydroxylation of benzene with H₂O₂, and phenol was detected as the main product in all the reactions (Table 5). Although there are small changes in the yields of phenol, they are consistent with the first oxidation events presumed to be Fe^IFe^I/Fe^{II}Fe^I for **I-V** which are at ca. 0.93 V, -0.11 V, 0.38 V, 0.14 V and 0.28 V respectively as shown in the CVs (Figure 6). From the infrared spectra (Figure 2) we can observe the ν_{CO} of complexes **III**, **IV** and **V** are little different due to the similar electron densities of Fe–Fe, which should be consistence with their almost similar activity of hydroxylation of benzene. It is notable that, for complex **II**, the bridging ligand, [I_{Me}(CH₂)₂I_{Me}] reduced the flexibility of di-iron complex and hindered the rotation of subunits which against H₂O₂ attack Fe–Fe bond to form the oxygen-transfer intermediate²⁴. On the other hand, although the increasing effect of electron donor due to the disubstituted ligands should

enhance its catalytic ability, but the effect of steric hindrance of bridging ligands overcome the effect of electron donor. Therefore, the yield of phenol catalyzed by complex **II** increased little.

Table 5. Effects of different catalysts and oxidants on hydroxylation of benzene to phenol^[a]

Entry	Catalyst	Catalyst(mmol)	Oxidant	Yield (%)
5 ⁷	I	0.05	H ₂ O ₂	7.5
6	I	0.01	H ₂ O ₂	0
7	II	0.01	H ₂ O ₂	26.7
8	III	0.01	H ₂ O ₂	23.4
9	V	0.01	H ₂ O ₂	24.3
10	FeSO ₄	0.01	<i>m</i> -CPBA	0

[a] catalyst; benzene, 0.1 mL; CH₃CN, 2.0 mL; oxidant 6.0 mmol; 60 °C; 3 h.

To our surprise, for the hydroxylation of benzene to phenol with *m*-CPBA by FeSO₄ no phenol was detected by gas chromatography (GC) under the same experimental conditions (Table 5 and Figure S12). Therefore, we inferred that the mechanism of hydroxyl radical oxidation for hydroxylation of benzene to phenol maybe ruled out here. DFT calculations carried out by Darensbourg²⁴ state that iron-based oxygenated product, Fe^{II}-(μ -O)-Fe^{II}, is more stable than S-oxygenated product, this indicates that Fe^{II}-(μ -O)-Fe^{II} isomer is thermodynamically favored in the diiron model complexes. Hence, we infer that the Fe^{II}-(μ -O)-Fe^{II} active intermediate may be more likely to be capable to transfer oxygen atom to aromatic substrates in the process of hydroxylation. Although the isolation of the Fe^{II}-(μ -O)-Fe^{II} species based on our di-iron complexes have not be achieved to date, the Fe-(μ -O)-Fe sites in Fe/ZSM-35 as the oxygen transfer species in the catalytic oxidation has been identified by C. Li' group by *in situ* resonance Raman spectroscopy²⁵. Mechanism for the hydroxylation of benzene was proposed based on the theoretical and experimental results by our previous work⁷, which suggests that the reaction involves an electrophilic addition process between the Fe^{II}-(μ -O)-Fe^{II} species and benzene substrate. Combined with the electrophilic addition process, a further hydrogen-atom shift occurs, and then the oxygen atom is transferred to the substrates.

Conclusions

Four new monodentate and bidentate NHC-containing iron complexes **II-V** were synthesized by facile carbonyl replacement on the parent complex **I** in THF at room temperature. The X-ray crystallographic reveals that monodentate NHC ligands in **IV** is coordinated to one of the two Fe atoms and located in a basal position. Whereas, the chetaled bidentate ligand $I_{Me}(CH_2)_2I_{Me}$ in **II** is connected to the two Fe atoms with a symmetrically substituted cisoid basal/basal coordination pattern. It is worth pointing out that all of the four complexes have been found to be catalysts for proton reduction to hydrogen under electrochemical conditions conformed that the more δ -donating of NHC the much easier for reduction. The reduction potential of the novel model complex **II** at ca. -2.57 V is more negative than the other diiron complexes we have known. The electrocatalytic mechanism for proton reduction to H_2 by [Fe-Fe]-NHC will be investigated in our further studies. In addition, these complexes as homogeneous catalyst used for the hydroxylation of benzene to phenol with the maximum phenol yield of 26.7% are correlation with their initial potential of oxidation events.

Experimental Section

General Comments. Some reactions and operations were carried out using standard Schlenk and vacuum-line techniques under an atmosphere of nitrogen. All solvents and reagents were purchased from Guangfu Chemical and Sigma-Aldrich, respectively. The $Fe(CO)_5$ was obtained as a gift from Jiangsu Tianyi Ultra-fine Metal Powder Co., Ltd (China). Solvents were dried and distilled prior to use according to the standard methods. The purified solvents were stored with molecular sieves under N_2 for no more than 1 week before use. THF, hexane, CH_2Cl_2 , toluene and acetonitrile were stirred over molecular sieves under N_2 for 24 h prior to further purification. THF and hexane were distilled from sodium/benzophenone. Acetonitrile were distilled from NaH. All the solvents were deoxygenated before every use.

The NMR spectra were measured on a Bruker AVANCE III 400 MHz NMR spectrometer. 1H NMR and ^{13}C NMR shifts are referenced to residual solvent resonances according to literature values. Solution IR spectra were recorded on a

Shimadzu FTIR-8400 spectrometer using 0.1 mm KBr sealed cells. Elemental analysis was carried out on a Heraeus CHN-Rapid, fully automatic elemental analyzer with TCD detection, type: TMT CHN, BESTELL–NR 2215001.

Preparation of $I_{Me}(CH_2)_2I_{Me}\cdot 2HBr$ (1). A solution of 1-methylimidazole (2.49 g, 30 mmol) and 1,2-dibromoethane (2.82 g, 15 mmol) in CH_3CN (20 mL) was refluxed for 72 h under an atmosphere of nitrogen. The precipitate was filtered after cooling through a double-ended needle, and washed with THF (3×10 mL). Drying in vacuo, product **1** was given as white, hygroscopic powder (4.96 g, 93.9%). The bromide salt must be stored under an atmosphere of nitrogen in a dryer due to its easy deliquescence. 1H NMR (400 MHz, D_2O): δ = 3.962 ($2CH_3-$), 4.825 ($-CH_2CH_2-$), 7.501 ($2CH_3NCH=CHN$), 7.562 ($2CH_3NCH=CHN$), 8.840 ($2NCHN$).

Preparation of $IMes\cdot HCl$ (2). Glyoxylaldehyde (40%, 6.27 g, 43.21 mmol) with 50 mL anhydrous alcohol were added dropwise over 1 h to the anhydrous alcohol (50 mL) solution of 2,4,6-trimethylaniline (4.63 g, 33.57 mmol). The mixture was stirred at room temperature for 12 h and then a yellow solid was separated out, the insoluble material was filtered and then washed with cold alcohol, after dried in vacuum, gave 3.01 g yellow solid of N,N' -(ethane-1,2-diylidene) bis(2,4,6-trimethylaniline) (imine) in 61.5% yield.

In a flask, the above imine (1.50 g, 5.13 mmol) was dissolved in THF (12.5 mL), followed by dropwise addition of chloromethyl ethyl ether (0.612 g, 6.15 mmol), the mixture was stirred under N_2 at 40 °C for 18 h. The precipitate was filtered after cooling, and washed with ethyl ether (2×20 mL). The residue was dissolved in anhydrous alcohol as little as possible, and then ethyl ether (25 mL) was added to extract. Repeated the above operation until a white solid was obtained. The white solid was dried under vacuum affording salt **2** (0.95 g, 54.1%).

Preparation of $IMe\cdot HI$ (3). Methylimidazole (10.2 g, 0.125 mol) and iodomethane (17.8 g, 0.125 mol) were dissolved in 100 mL toluene and stirred at reflux for 12 h under an atmosphere of nitrogen. After cooling to room temperature toluene was filtered off through a double-ended needle then a white solid was formed. The residue was dissolved in anhydrous alcohol as little as possible, and then ethyl ether (50 mL) was added to extract. Repeated the above operation until a white solid was obtained. The white solid was dried in vacuo to yield 27.2 g (97.1%) of **3**. The same as $I_{Me}(CH_2)_2I_{Me}\cdot 2HBr$, $IMe\cdot HI$ must be stored under an atmosphere of nitrogen in a dryer.

Preparation of $(\mu\text{-dmedt})Fe_2(CO)_6$ (I). $Fe(CO)_5$ (13.4 g, 68.6 mmol) and 2,3-butanedithiol (2.77 g, 22.7 mmol) were

added to 55 mL toluene and stirred at reflux for 29 h under an atmosphere of nitrogen. Then the solvent were distilled under 140 °C, and the residue were dissolved in little toluene and loaded onto a silica gel column. The product was then eluted with hexane. Solvent was evaporated from the dark red eluant to yield a red powder of **I** (3.439 g, 37.9%). IR (CH₂Cl₂) ν_{CO} = 2073, 2032, 2000, 1990 cm⁻¹. ¹H NMR (400 MHz, CDCl₃) δ = 2.24(s, CH=CH), 1.36(m, CH₃C-CCH₃). ¹³C NMR (400 MHz, CDCl₃) δ = 208.63 (CO); 55.21 and 49.37 (SCH(CH₃)CH(CH₃)CHS); 20.61 and 19.14 (SCH(CH₃)CH(CH₃)CHS). Elemental analysis: Calc. for C₁₀H₈O₆Fe₂S₂: C, 30.03; H, 2.02. Found: C, 30.11; H, 2.01.

Preparation of (μ -dmedt)Fe₂(CO)₄(I_{Me}(CH₂)₂I_{Me}) (II**) and [(μ -dmedt)Fe₂(CO)₅]₂ (I_{Me}(CH₂)₂I_{Me}) (**III**).**

I_{Me}(CH₂)₂I_{Me}·2HBr (160 mg, 0.46 mmol) was dried in vacuo under N₂ for 30 min in a 50 mL Schenk flask, then *t*-BuOK (184 mg, 1.64 mmol) and THF (7 mL) were added to the mixture after dried in vacuo under N₂ for 20 min. After 3 h of vigorous stirring at room temperature, a THF (7 mL) solution of **I** (77 mg, 0.23 mmol) was transferred to the reaction mixture over 35 min by a double-ended needle at room temperature. The resulting mixture was stirred at room temperature for 1.25 h, monitoring by IR spectroscopy to confirm that the reaction had reached completion. The solution was evaporated to dryness in vacuo. The resulting red solid was dissolved in a minimum amount of CH₂Cl₂ and applied to an aluminum oxide column. The first red band was eluted with a CH₂Cl₂/hexane (1/2) mixture. Slow evaporation of the solvent gave an orange powder of **III** (26 mg, 29.0%). A second red band eluted with CH₂Cl₂/hexane (1/1) gave a red powder of complex **II** (11 mg, 12.4%) after slow evaporation of the solvents.

Complex **II**: IR (CH₂Cl₂) ν_{CO} = 1961, 1924, 1886 cm⁻¹. ¹H NMR(400 MHz, Acetone-d₆) δ = 7.11-6.98 (m, 2 NCH=CHN), 5.85-5.43 (m, NCH₂CH₂N), 4.29 (m, NCH₂CH₂N), 3.95 (d, 2 NCH₃), 2.29 (m, SCH(CH₃)CH(CH₃)S), 1.94 (m, SCH(CH₃)CH(CH₃)S), 1.47 (d, SCH(CH₃)CH(CH₃)S), 1.26 (d, SCH(CH₃)CH(CH₃)S). ¹³C NMR (400 MHz, Acetone-d₆) δ = 222.32, 221.61 and 216.47 (CO); 188.95 (C_{carbene}); 123.76, 123.40, 122.98 and 122.06 (NCH=CHN); 54.90 and 54.57 (NCH₂CH₂N); 47.10 and 46.49 (NCH₃); 39.09 and 38.85 (SCH(CH₃)CH(CH₃)CHS); 20.70 and 20.35 (SCH(CH₃)CH(CH₃)CHS). Elemental analysis: Calc. for C₁₈H₂₂O₄N₂Fe₂S₂: C, 40.47; H, 4.15; N, 10.49. Found: C, 40.34; H, 4.14; N, 10.52.

Complex **III**: IR (CH₂Cl₂) ν_{CO} =2040, 2034, 1973, 1905 cm⁻¹. ¹H NMR(400 MHz, CD₂Cl₂) δ = 7.11 (m, 2 NCH=CHN), 6.24 (m, NCH₂CH₂N), 4.05 (d, 2 NCH₃), 2.06 (m, SCH(CH₃)CH(CH₃)S), 0.92 (d, SCH(CH₃)CH(CH₃)S). Elemental analysis: Calc. for C₂₈H₃₀O₁₀N₄Fe₄S₄: C, 36.00; H, 3.24; N, 6.00. Found: C, 36.12; H, 3.23; N, 6.01.

Preparation of (μ -dmedt)Fe₂(CO)₅(IMes) (IV). Solid **I** (93 mg, 0.23 mmol) and salt **2** (198 mg, 0.58 mmol) were combined, dried in vacuo for 30 min and then dissolved in THF (4.5 mL). After stirring for another 30 min, the previously dried *t*-BuOK (130 mg, 1.16 mmol) in 3.5 mL of THF was added, and the resulting mixture was stirred for an additional 30 min, monitoring by IR spectroscopy to confirm that the reaction had reached completion. The solvent was then removed, and the red residue were dissolved in CH₂Cl₂ and loaded onto a silica gel column. Elution with petroleum ether removed excess starting material **I**. The product was then eluted with CH₂Cl₂. Solvent was evaporated from the dark red eluant to yield product **IV** (140 mg, 89%). IR (CH₂Cl₂) ν_{CO} =2036, 2028, 1971, 1909 cm⁻¹. ¹H NMR(400 MHz, Acetone-d₆) δ = 7.46 and 7.36 (s, NCH=CHN); 7.08 and 7.06 (d, ArH); 2.35 (s, p-ArCH₃); 2.21-2.16 (m, o-ArCH₃); 1.79 (m, SCH(CH₃)CH(CH₃)S); 1.04-0.92 (m, SCH(CH₃)CH(CH₃)S). ¹³C NMR (400 MHz, Acetone-d₆) δ = 216.02, 212.43 and 211.88 (CO); 187.48 (C_{carbene}); 138.99, 137.93, 136.06 (C₆H₂); 128.94 and 125.65 (NCH=CHN); 53.58 and 47.65 (SCH(CH₃)CH(CH₃)CHS); 20.23, 19.89, 19.43, 18.42, 18.14, 18.03 and 17.83 (CH₃). Elemental analysis: Calc. for C₃₀H₃₂O₅N₂Fe₂S₂: C, 53.27; H, 4.78; N, 4.14. Found: C, 53.13; H, 4.79; N, 4.15.

Preparation of (μ -dmedt)Fe₂(CO)₅(IMe) (V). Complex **V** was prepared by a procedure similar to that of **IV** from IMe·HI (585 mg, 2.61 mmol), **I** (1.00 g, 2.50 mmol) and *t*-BuOK (569 mg, 5.07 mmol). The product was obtained as orange solid: yield 1.01g, 86.1%. IR (CH₂Cl₂) ν_{CO} = 2038, 2032, 1971, 1911cm⁻¹. ¹H NMR(400 MHz, CD₃CN) δ = 7.14 (s, NCH=CHN); 3.94 (s, NCH₃); 2.03 (s, SCH(CH₃)CH(CH₃)S), 1.23 (m, broad, SCH(CH₃)CH(CH₃)S), 0.88 (s, broad, SCH(CH₃)CH(CH₃)S). ¹³C NMR (400 MHz, CD₃CN) δ = 217.40 and 212.08 (CO); 163.52 (C_{carbene}); 124.07 and 120.01 (NCH=CHN); 55.11 (NCH₃); 39.16 (SCH(CH₃)CH(CH₃)CHS); 20.07 (CH₃). Elemental analysis: Calc. for C₁₄H₁₆O₅N₂Fe₂S₂: C, 35.92; H, 3.45; N, 5.98. Found: C, 36.02; H, 3.46; N, 5.96.

X-ray Crystallography. The single-crystal X-ray diffraction data were collected with a Rigaku MM-007 diffractometer equipped with a Saturn 724CCD. Data were collected at 293 K or 113 K using a confocal monochromator with Mo-K α radiation (λ =0.71073 Å). Data collection, reduction and absorption correction were performed with the CRYSTALCLEAR program²⁶. Structure was solved by direct methods using the SHELXS-97 program²⁷ and refined by full-matrix least-squares techniques (SHELXL-97)²⁸ on F^2 . Hydrogen atoms were located by geometrical calculation. Details of crystal data, data collections and structure refinements are summarized in Table S1 and Figure S1-S3.

Cyclic Voltammograms. Cyclic voltammograms were obtained in a three-electrode cell under N₂ using a CHI 660B

electrochemical workstation. The working electrode was a glassy carbon disk (diameter 3 mm) polished with 3 and 1 μm diamond pastes and sonicated in ion-free water for 20 min prior to use. The reference electrode was a non-aqueous Ag/Ag^+ (in a CH_3CN solution of 0.01 M $\text{AgNO}_3/0.1$ M $n\text{-Bu}_4\text{NPF}_6$) electrode and the counter electrode was platinum wire. A solution of 0.1 M $n\text{-Bu}_4\text{NPF}_6$ in CH_3CN was used as supporting electrolyte, which was degassed by bubbling with dry N_2 for 10 min before measurement. Ferrocene was used as an internal standard under the same measuring conditions and all potentials were referenced to the $\text{Cp}_2\text{Fe}^+/0$ couple at 0 V. During the electrocatalytic experiments under N_2 , increments of glacial HOAc (chromatographic grade, $\cong 99.8\%$, water 0.15%, by Karl Fischer method) were added by microsyringe.

Catalytic Hydroxylation. Hydroxylation of benzene with H_2O_2 (30%, w/w, in H_2O) was carried out in a 25 mL round bottom flask equipped with a reflux condenser and a magnetic stirrer. In a typical reaction, **IV** (7 mg, 0.01 mmol) was dissolved in CH_3CN (2.0 mL). After the mixture was heated to the desired temperature, benzene (0.1 mL, 1.1 mmol) was added to the mixture. A certain amount of H_2O_2 was added at last to start the reaction and the mixture was stirred for several hours. All the experiments were conducted at ambient pressure. Measurements of GC (9890B) equipped with a FID detector and a capillary column (OV-1701; 30 m \times 0.25 mm \times 0.25 μm) were performed to analyze the product mixture. Internal standard method was used to quantitative analysis and chlorobenzene was chosen as the internal standard substance. TPD analysis was carried out, from 80 $^\circ\text{C}$ to 200 $^\circ\text{C}$ by a ramp of 10 $^\circ\text{C}$, then from 200 $^\circ\text{C}$ to 280 $^\circ\text{C}$ by a ramp of 30 $^\circ\text{C}$. This reaction system appeared to have a high selectivity since phenol was the only product detected by GC.

Supporting Information

X-ray structural data for **II** (CCDC 1035522) and **IV** (CCDC 1035526), electrochemistry, and GC Figures are included.

Acknowledgements

We are grateful to the National Natural Science Foundation of China (21103121 and 21276187), the Research Fund for the Doctoral Program of Higher Education of China (20110032120011) and the Tianjin Municipal Natural Science Foundation (13JCQNJC05800) for financial support of this work.

References

1. a) Z. Xiao, Z. Wei, L. Long, Y. Wang, D. J. Evans and X. Liu, *Dalton Trans.* 2011, **40**, 4291-4299; b) P. Li, M. Wang, C. He, G. Li, X. Liu, C. Chen, B. Åkermark and L. Sun, *Eur. J. Inorg. Chem.* 2005, **2005**, 2506-2513; c) B.-E. Jugder, J. Welch, K.-F. Aguey-Zinsou, C. P. Marquis, *RSC Advances* 2013, **3**, 8142-8159.
2. a) E. J. Lyon, I. P. Georgakaki, J. H. Reibenspies and M. Y. Darensbourg, *Angew. Chem. Int. Ed.* 1999, **38**, 3178-3180; b) A. L. Cloirec, S. P. Best, S. Borg, S. C. Davies, D. J. Evans, D. L. Hughesa and C. J. Pickett, *Chem. Commun.* 1999, 2285-2286.
3. a) R. Lopes, J. M. S. Cardoso, L. Postigo and B. Royo, *Catal. Lett.* 2013, **143**, 1061-1066; b) C. d. Tard and C. J. Pickett, *Chem. Rev.* 2009, **109**, 2245-2274; c) C. Cao, Y. Zhuang, J. Zhao, H. Liu, P. Geng, G. Pang and Y. Shi, *Synth. Commun.* 2012, **42**, 380-387; d) M. Lee, Z. Niu, D. V. Schoonover, C. Slebodnick and H. W. Gibson, *Tetrahedron* 2010, **66**, 7077-7082.
4. a) F. Godoy, C. Segarra, M. Poyatos and E. Peris, *Organometallics* 2011, **30**, 684-688; b) D. Morvan, J. F. Capon, F. Gloaguen, G. A. Le, M. Marchivie, F. Michaud, P. Schollhammer, J. Talarmin, J. J. Yaouanc, R. Pichon and N. Kervarec, *Organometallics* 2007, **26**, 2042-2052; c) L. Merces, G. Labat, A. Neels, A. Ehlers and M. Albrecht, *Organometallics* 2006, **25**, 5648-5656; d) J. F. Capon, S. E. Hassnaoui, F. Gloaguen, P. Schollhammer and J. Talarmin, *Organometallics* 2005, **24**, 2020-2022.
5. a) C. M. Thomas, T. Liu, M. B. Hall and M. Y. Darensbourg, *Inorg. Chem.* 2008, **47**, 7009-7024; b) J. Wu, W. Dai, J. H. Farnaby, N. Hazari, J. J. Le Roy, V. Mereacre, M. Murugesu, A. K. Powell and M. K. Takase, *Dalton Trans.* 2013, **42**, 7404-7413; c) X. Wang, Z. Mo, J. Xiao and L. Deng, *Inorg. Chem.* 2013, **52**, 59-65; d) M. J. Ingleson and R. A. Layfield, *Chem. Commun.* 2012, **48**, 3579-3589; e) S. Zlatogorsky, C. A. Muryn, F. Tuna, D. J. Evans and M. J. Ingleson, *Organometallics* 2011, **30**, 4974-4982.
6. E. S. Donovan, G. S. Nichol and G. A. N. Felton, *J. Organomet. Chem.* 2013, **726**, 9-13.
7. X. Wang, T. Y. Zhang, Q. S. Yang, S. Jiang and B. Li, *Eur. J. Inorg. Chem.* 2015, **5**, 817-825.
8. J. Louie and R. H. Grubbs, *Chem. Commun.* 2000, 1479-1480.
9. a) A. Volkov, E. Buitrago and H. Adolfsson, *Eur. J. Org. Chem.* 2013, **11**, 2066-2070; b) S. Demir, Y. Gökçe, N. Kaloğlu, J. B. Sortais, C. Darcel and İ. Özdemir, *Appl. Organomet. Chem.* 2013, **27**, 459-464; c) T. Hashimoto, S. Urban, R. Hoshino, Y. Ohki, K. Tatsumi and F. Glorius, *Organometallics* 2012, **31**, 4474-4479; d) D. Bézier, G. T. Venkanna, J. B. Sortais and C. Darcel, *ChemCatChem* 2011, **3**, 1747-1750.
10. a) C. Pranckevicius and D. W. Stephan, *Organometallics* 2013, **32**, 2693-2697; b) T. Hatakeyama, S. Hashimoto, K.

- Ishizuka and M. Nakamura, *J. Am. Chem. Soc.* 2009, **131**, 11949-11963; c) T. Yamagami, R. Shintani, E. Shirakawa and T. Hayashi, *Org. Lett.* 2007, **9**, 1045-1048.
11. a) C. M. Guisan, F. Tato, E. Bunuel, P. Calle and D. J. Cardenas, *Chem. Sci.* 2013, **4**, 1098-1104; b) J. A. Przyojski, H. D. Arman and Z. J. Tonzetich, *Organometallics* 2012, **31**, 3264-3271; c) L. Xiang, J. Xiao and L. Deng, *Organometallics* 2011, **30**, 2018-2025.
12. a) Y. S. Wang, H. M. Sun, X. P. Tao, Q. Shen and Y. Zhang, *Chin. Sci. Bull.* 2007, **52**, 3193-3199; b) M. Z. Chen, H. M. Sun, W. F. Li, Z. G. Wang, Q. Shen and Y. Zhang, *J. Organomet. Chem.* 2006, **691**, 2489-2494.
13. a) X. Li, M. Wang, D. Zheng, K. Han, J. Dong and L. C. Sun, *Energy Environ. Sci.* 2012, **5**, 8220-8224; b) F. Wang, W. G. Wang, X. J. Wang, H. Y. Wang, C. H. Tung and L. Z. Wu, *Angew. Chem. Int. Ed.* 2011, **50**, 3193-3197; c) M. L. Singleton, J. H. Reibenspies and M. Y. Darensbourg, *J. Am. Chem. Soc.* 2010, **132**, 8870-8871.
14. a) S. Zhu, R. Liang, L. Chen, C. Wang, Y. Ren and H. Jiang, *Tetrahedron Lett.* 2012, **53**, 815-818; b) T. Schaub, M. Backes and U. Radius, *Organometallics* 2006, **25**, 4196-4206.
15. L. C. Song, C. G. Li, J. H. Ge, Z. Y. Yang, H. T. Wang, J. Zhang and Q. M. Hu, *J. Inorg. Biochem.* 2008, **102**, 1973-1979.
16. L. C. Song, X. Luo, Y. Z. Wang, B. Gai and Q. M. Hu, *J. Organomet. Chem.* 2009, **694**, 103-112.
17. J. D. Lawrence, T. B. Rauchfuss and S. R. Wilson, *Inorg. Chem.* 2002, **41**, 6193-6195.
18. X. Zhao, I. P. Georgakaki, M. L. Miller, J. C. Yarbrough and M. Y. Darensbourg, *J. Am. Chem. Soc.* 2001, **123**, 9710-9711.
19. P. Buchgraber, L. Toupet, and V. Guerschais, *Organometallics* 2003, **22**, 5144-5147.
20. M. L. Singleton, R. M. Jenkins, C. L. Klemashevich and M. Y. Darensbourg, *C. R. Chimie* 2008, **11**, 861-874.
21. J. F. Capon, S. Ezzaher, F. Gloaguen, F. Y. Pétillon, P. Schollhammer, J. Talarmin, T. J. Davin, J. E. McGrady and K. W. Muir, *New J. Chem.* 2007, **31**, 2052-2064.
22. a) T. Liu and M. Y. Darensbourg, *J. Am. Chem. Soc.* 2007, **129**, 7008-7009; b) J. W. Tye, J. Lee, H. W. Wang, R. R. Mejia, Joseph H. Reibenspies, M. B. Hall and M. Y. Darensbourg, *Inorg. Chem.* 2005, **44**, 5550-5552.
23. a) L. C. Song, J. H. Ge, X. G. Zhang, Y. Liu and Q. M. Hu, *Eur. J. Inorg. Chem.* 2006, **2006**, 3204-3210; b) L. C. Song, Z. Y. Yang, H. Z. Bian, Y. Liu, H. T. Wang, X. F. Liu and Q. M. Hu, *Organometallics* 2005, **24**, 6126-6135; c) R. R. Mejia, D. Chong, J. H. Reibenspies, M. P. Soriaga and M. Y. Darensbourg, *J. Am. Chem. Soc.* 2004, **126**, 12004-12014; d) D. Chong, I. P. Georgakaki, R. R. Mejia, C. J. Sanabria, M. P. Soriaga and M. Y. Darensbourg,

Dalton Trans. 2003, **21**, 4158-4163.

24. a) B. Li, T. B. Liu, M. L. Singleton, M. Y. Darensbourg, *Inorg. Chem.* 2009, **48**, 8393-8403; b) T. B. Liu, B. Li, M. L. Singleton, M. B. Hall, M. Y. Darensbourg, *J. Am. Chem. Soc.* 2009, **131**, 8296-8307.
25. J. Wang, G. Li, X. Ju, H. Xia, F. Fan, J. Wang, Z. Feng, C. Li, *J. Catal.* 2013, **301**, 77-82.
26. CRYSTALCLEAR 1.3.6. Rigaku and Rigaku/MSO (2005). 9009 New Trail Dr. The Woodlands TX 77381 USA.
27. Sheldrick, G. M. SHELXS-97, A Program for Crystal Structure Solution; University of Göttingen: Germany, 1997.
28. Sheldrick, G. M. SHELXL-97, A Program for Crystal Structure Refinement; University of Göttingen: Germany, 1997.